Supplementary materials

High-Efficiency TADF Materials Featuring Carbazole-Modified Spiroacridan-Pyrimidine Skeletons with an External Quantum Efficiency Exceeding 26% in Blue-Green Light Emission

Yi-Zhen Li,[1$] Fu-En Szu,[1$] Han-Yun Szu,[1] Chao-Che Wu,[2] Yong-Yun Zhang,[1] Zong-Huan Li,[a] Jiun-Haw Lee,[2*] Tien-Lung Chiu,[3*] and Man-kit Leung[1,4*]

[1]*Department of Chemistry, National Taiwan University, Taipei 10617, Taiwan.*

[2]*Graduate Institute of Photonics and Optoelectronics and Department of Electrical Engineering, National Taiwan University, Taipei 10617, Taiwan.*

[3]*Department of Electrical Engineering, Yuan Ze University, Chung-Li, Taoyuan 32003, Taiwan.*

[4]*Advanced Research Center for Green Materials Science and Technology, National Taiwan University, Taipei 10617, Taiwan.*

[$] *Yi-Zhen Li and Fu-En Szu contributed equally to this work.*

Email: jiunhawlee@ntu.edu.tw;tlchiu@saturn.yzu.edu.tw;mkleung@ntu.edu.tw

2-(3,4,5-trifluorophenyl)pyrimidine (**1**)

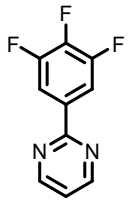

1

The procedure is followed by our previous report.[1] The NMR spectra are also presented in the ESI in the previous report.

A mixture of 2,4,5-trifluorophenylboronic acid (5.842 g, 33.21 mmol), 2-bromopyrimidine (3.5 g, 22.14 mmol), $Pd(OAc)_2$ (0.2485 g, 1.107 mmol) and triphenylphosphine (1.155 g, 4.428 mmol) was flushed with argon then methoxymethane (22 mL) and potassium carbonate solution (21 mL, 2.7 M, 56.7 mmol) were added respectively. The resulting mixture was refluxed at 105℃ for 2.5 hours. After the reaction, the solvent was removed by vacuum distillation. The residue was extracted with dichloromethane and water. The organic layer was dried over anhydrous $MgSO_4$ and removed under reduced pressure. The crude product was purified through column chromatography with dichloromethane and afforded compound **1** as a white solid (3.2970 g, 70% yield).

10-(2,6-difluoro-4-(pyrimidin-2-yl)phenyl)-10H-spiro[acridine-9,9'-fluorene] (**2**)

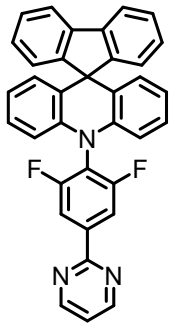

2

A mixture of compound **1** (1.7 g, 5.2 mmol), 10*H*-spiro[acridine-9,9'-fluorene] (1.0 g, 4.8 mmol), and Cs_2CO_3 (2.3 g, 7.1 mmol) in 4.8 mL dimethyl sulfoxide (DMSO) were refluxed at 200°C under argon for 15h. After the reaction, the solvent was removed by vacuum distillation. The residue was dissolved in dichloromethane and extracted by water and saturated NaCl solution. The organic layer was dried by anhydrous $MgSO_4$. The crude was further purified through chromatography with hexanes/ dichloromethane mixtures 1:2 (v/v) as eluent to afford the purified product (1.6 g, 65%) as a yellow solid. ^{1}H NMR (400 MHz, DMSO-d_6): δ 9.01 (d, *J*= 4.8 Hz, 2 H), 8.38 (d, *J*= 9.2 Hz, 2 H), 7.94 (d, *J*= 7.6 Hz, 2 H), 7.59 (t, *J*= 4.8 Hz, 1 H), 7.38 (t, *J*= 7.6 Hz, 2 H), 7.31 (d, *J*= 7.2 Hz, 2 H), 7.25 (t, *J*= 7.2 Hz, 2 H), 7.01 (t, *J*= 7.2 Hz, 2 H), 6.64 (t, *J*= 7.2 Hz, 2 H), 6.46 (d, *J*= 8.0 Hz, 2 H), 6.26 (d, *J*= 7.6 Hz, 2 H); ^{13}C NMR (100 MHz, DMSO-d_6): δ 162.09, 162.05, 161.86, 160.59, 159.60, 159.55, 158.19, 155.54, 140.83, 138.90, 138.80, 128.60, 128.20, 128.02, 127.40, 125.15, 125.02, 121.78, 121.27, 120.51, 117.99, 117.81, 117.63, 113.35, 112.66, 112.43, 109.49, 56.08; HR-FAB m/z calcd for $C_{35}H_{21}F_2N_3$ (M^+) 521.1704, obsd. 521.1710.

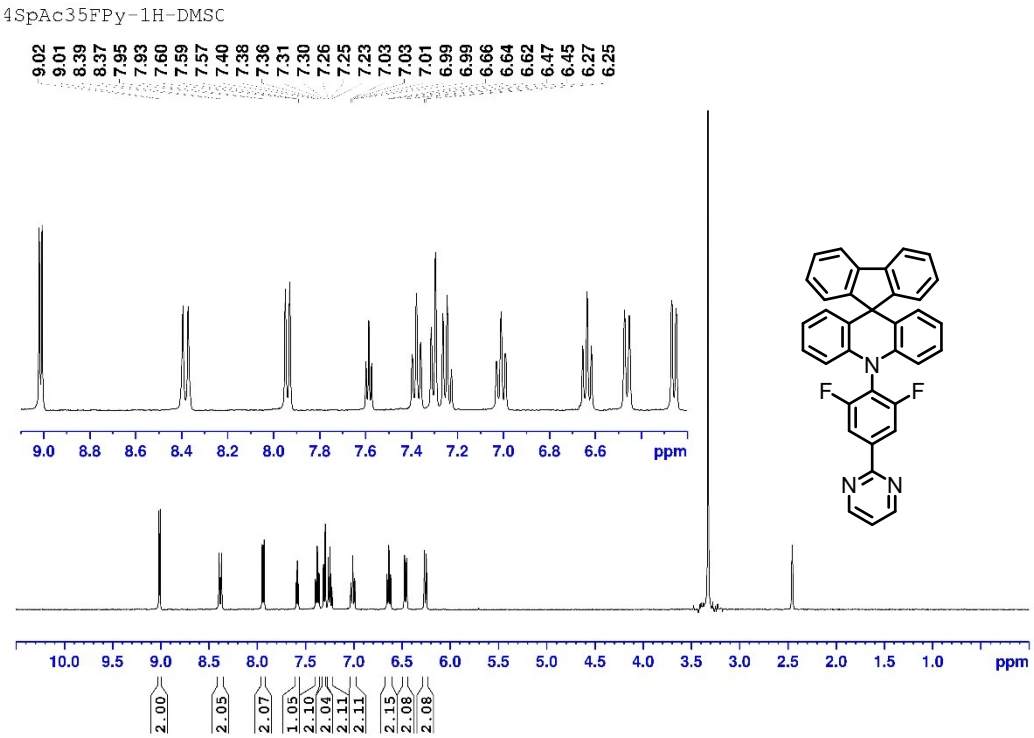

Fig. S1. ^{1}H NMR spectrum of compound (**2**).

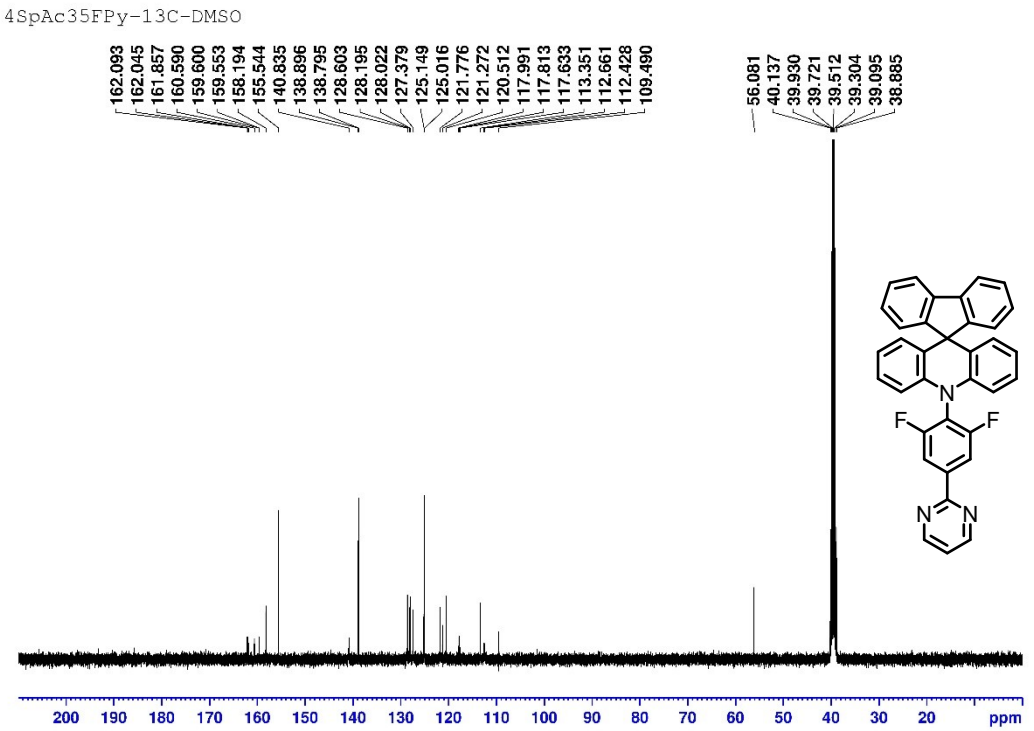

Fig. S2. ^{13}C NMR spectrum of compound (**2**).

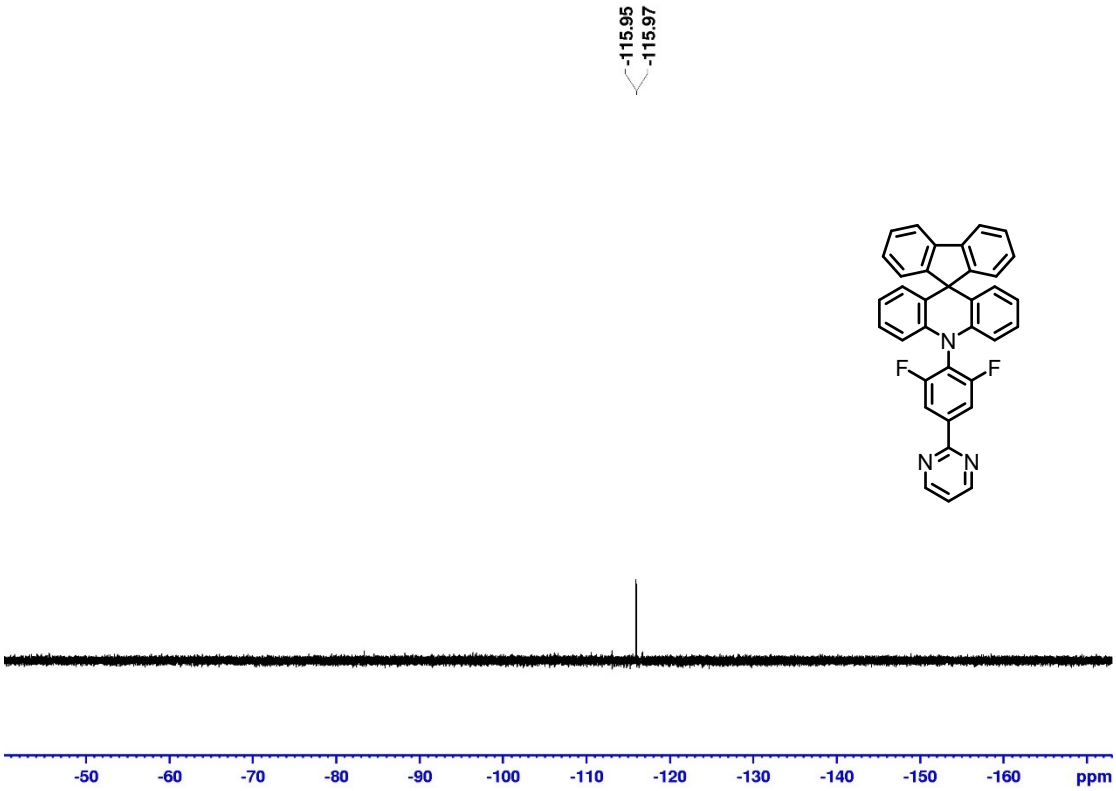

Fig. S3. ^{19}F NMR spectrum of compound (**2**).

10-(2,6-di(9H-carbazol-9-yl)-4-(pyrimidin-2-yl)phenyl)-10H-spiro[acridine-9,9'-fluorene] (**4SpAc35CzPy**)

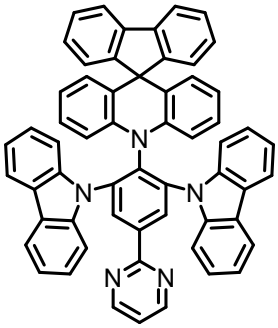

4SpAc35CzPy

A mixture of compound **2** (1.00 g, 1.91 mmol), carbazole (0.38 g, 2.29 mmol), and Cs_2CO_3 (0.91 g, 2.8 mmol) in 1.9 mL dimethyl sulfoxide (DMSO) were refluxed at 200°C under argon for 15h. After the reaction, the solvent was removed by vacuum distillation. The residue was dissolved in dichloromethane and extracted by water and saturated NaCl solution. The organic layer was dried by anhydrous $MgSO_4$. The crude was further purified through chromatography with hexanes/ dichloromethane mixtures 1:2 (v/v) as eluent to afford the purified product (1.1 g, 73%) as a yellow solid.

^{1}H NMR (400 MHz, DMSO-d_6): δ 9.03 (d, *J*= 4.8 Hz, 2 H), 9.00 (s, 2 H), 8.09 (d, *J*= 7.6 Hz, 4 H), 7.66 (d, *J*= 7.6 Hz, 2 H), 7.61 (t, *J*= 4.8 Hz, 1 H), 7.51 (d, *J*= 8.2 Hz, 4 H), 7.22 (d, *J*= 7.2 Hz, 4 H), 7.13 (t, *J*= 8.2 Hz, 6 H), 7.05 (d, *J*= 8.2 Hz, 2 H), 6.78 (t, *J*= 7.6 Hz, 2 H), 6.36 (t, *J*= 7.8 Hz, 2 H), 6.11 (t, *J*= 7.6 Hz, 2 H), 5.45 (dd, *J*= 8.2, 1.5 Hz, 2 H), 5.07 (d, *J*= 7.6 Hz, 2 H); ^{13}C NMR (100 MHz, Chloroform-d_1): δ 162.59, 158.66, 157.59, 140.53, 139.66, 139.23, 138.59, 137.00, 135.81, 130.85, 128.67, 128.07, 126.68, 126.15, 125.53, 125.27, 123.58, 123.13, 120.99, 120.13, 120.01, 119.95, 119.03, 115.47, 110.74, 54.89; HR-FAB m/z calcd for $C_{59}H_{37}N_5$ (M+) 815.3049 obsd. 815.3050.

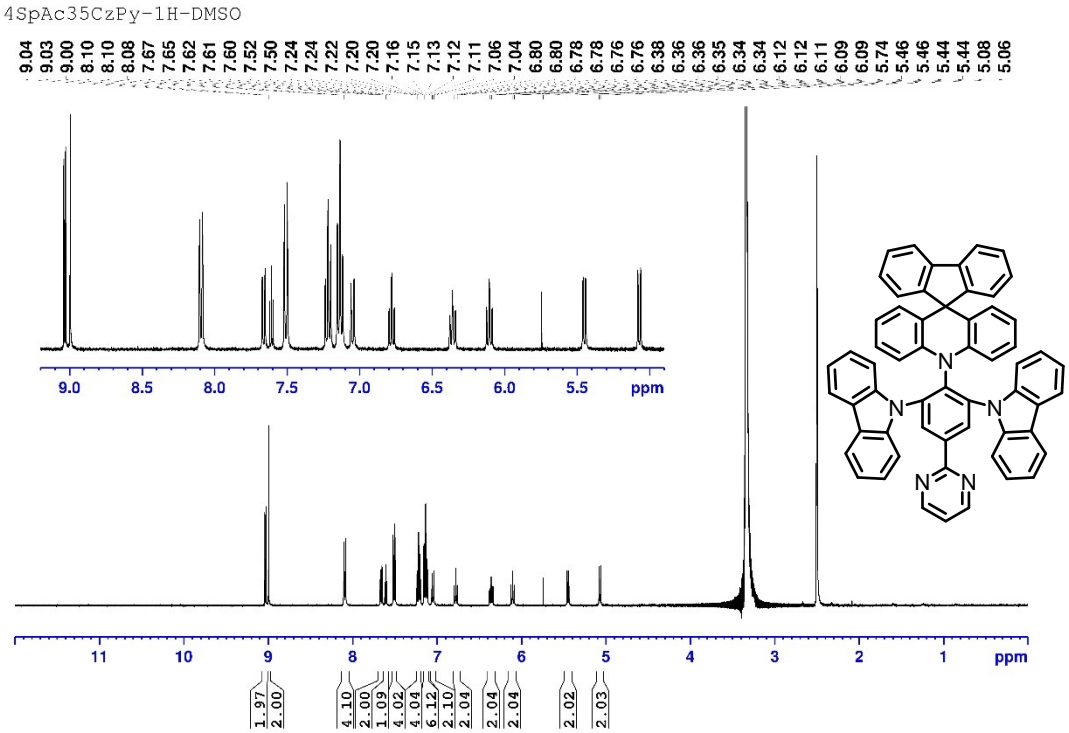

Fig. S4. ^{1}H NMR spectrum of **4SpAc35CzPy**.

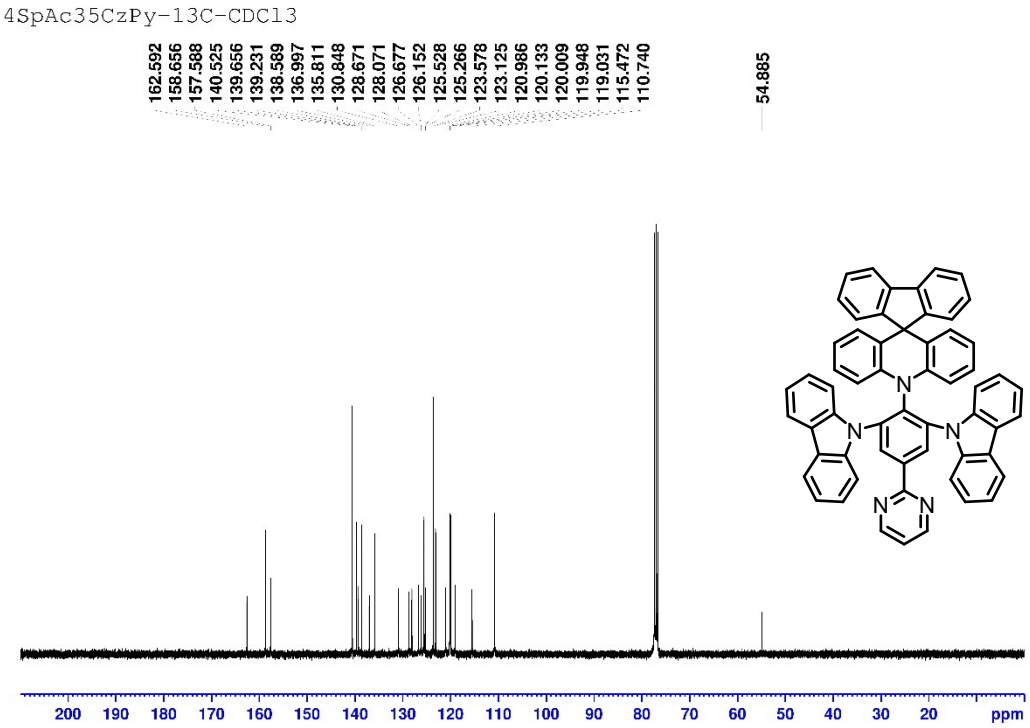

Fig. S5. ^{13}C NMR spectrum of **4SpAc35CzPy**.

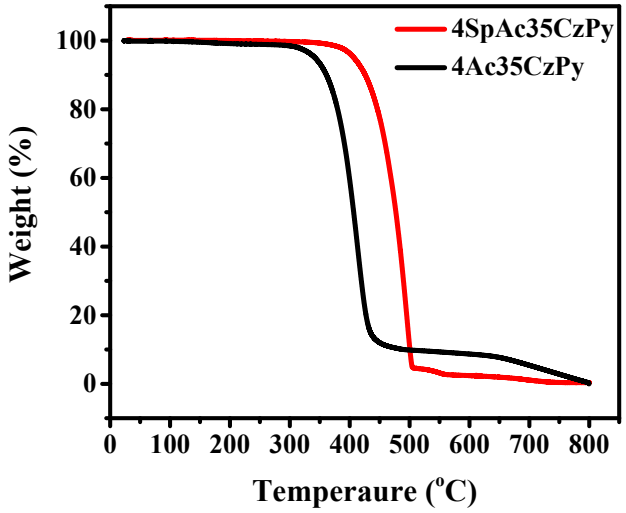

Fig. S6. Thermal gravity analysis (TGA) curves of **4SpAc35CzPy** and **4Ac35CzPy**.

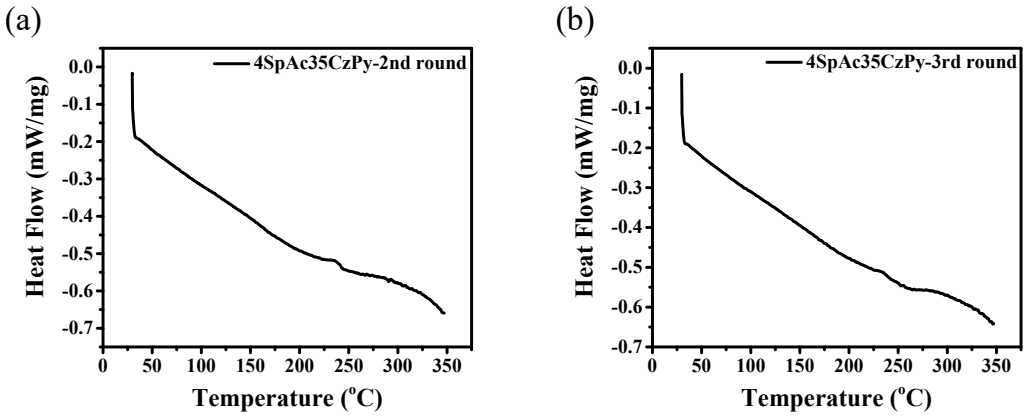

Fig. S7. Differential scanning calorimetry (DSC) curves of **4SpAc35CzPy**.

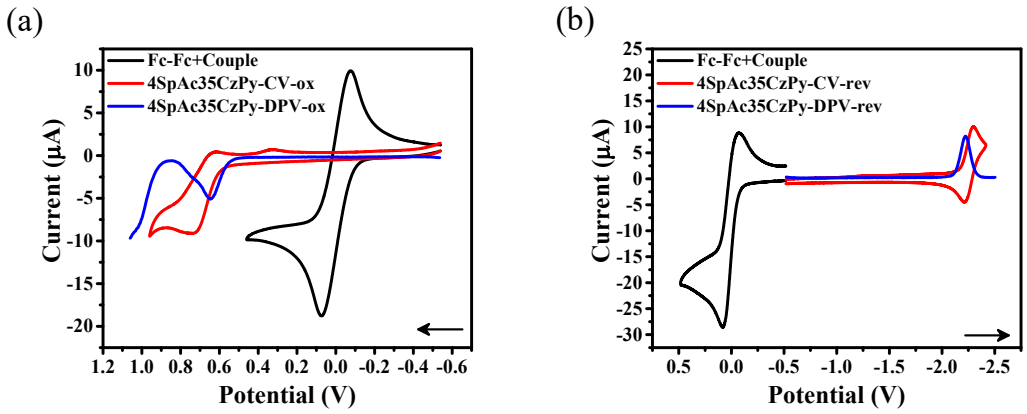

Fig. S8. Cyclic voltammogram (CV) and differential pulse voltammetry (DPV) of **4SpAc35CzPy** (a) oxidation and (b) reduction.

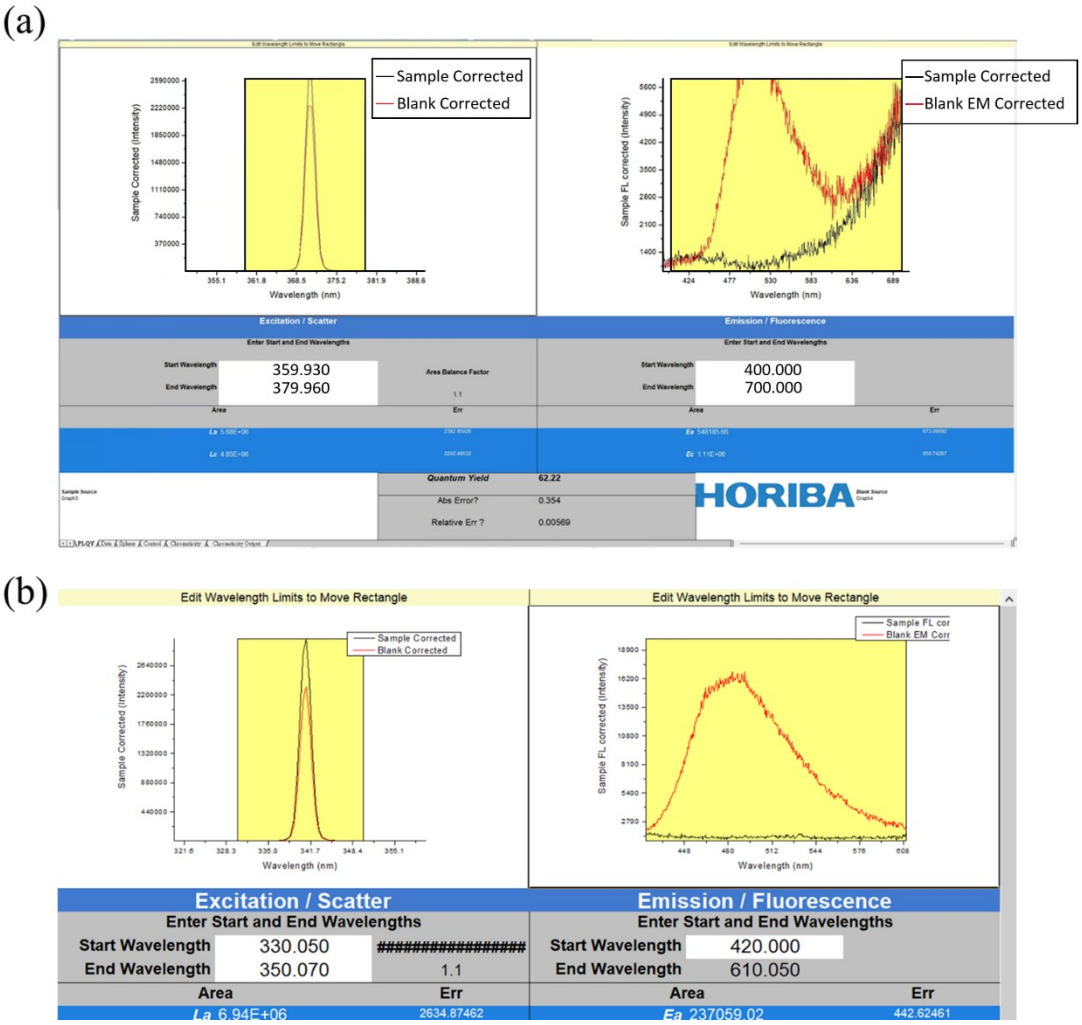

Fig. S9. PLQY of **4SpAc35CzPy** in (a) pristine thin film and (b) doped in ***o*-DiCbzBz** (15%).

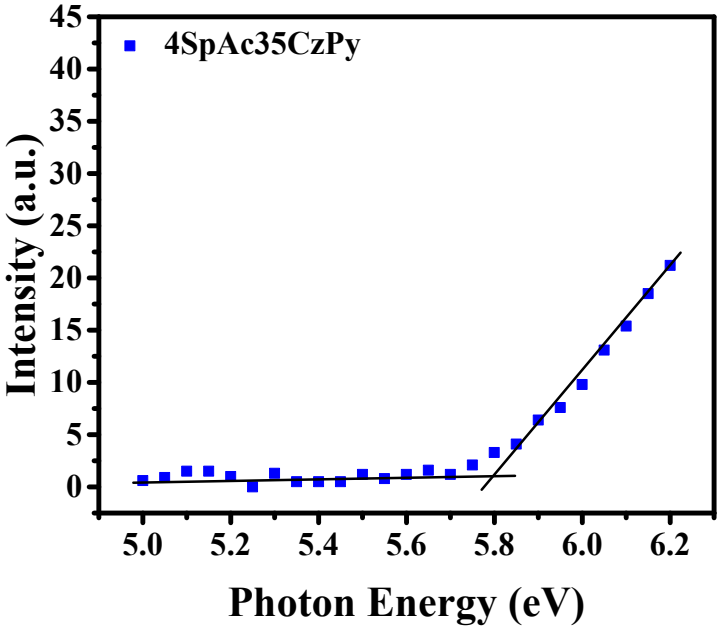

Fig. S10. Photoelectron spectrum of **4SpAc35CzPy**.

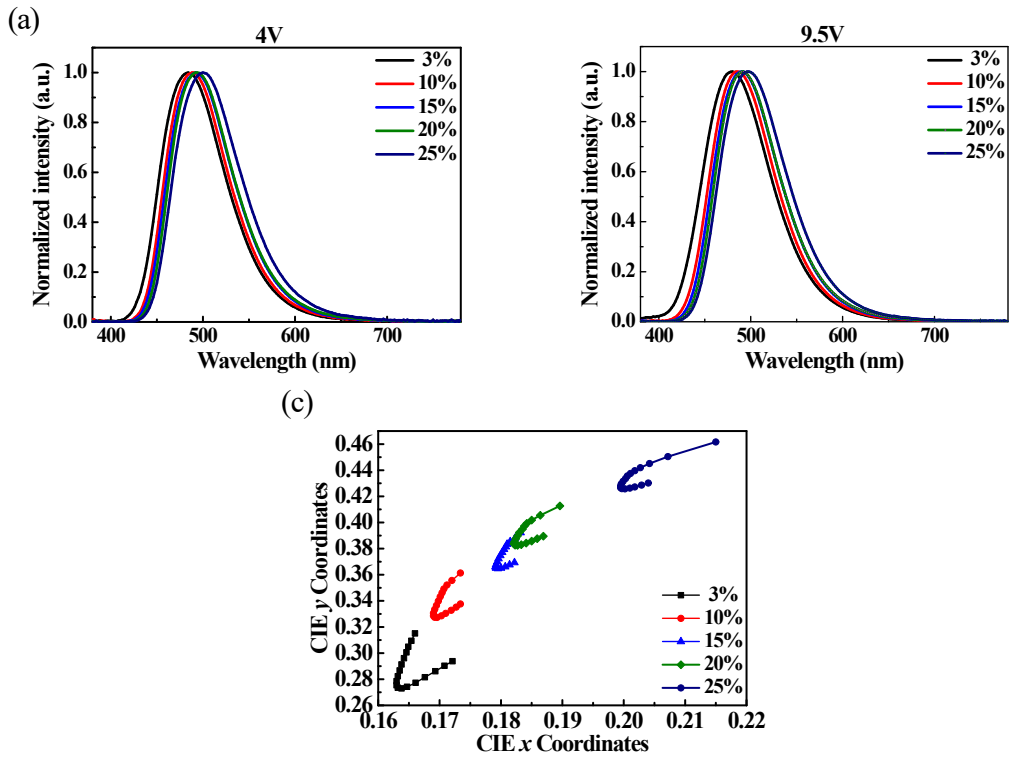

Fig. S11. The EL spectrum at (a) 4 V, (b) 9.5 V, and (c) CIE coordinates in various dopant concentrations.

Table S1. The device structure of OLEDs while **4SpAc35CzPy** with different dopant concentration, ETL, and EML thickness.

HTL TAPC	EBL *m*CP	EML *o*-DiCbzBz/ X% 4SpAc35CzPy	ETL DPPS	cathode LiF/Al
		30 /3%		
		30 /10%		
		30 /15%	55	
		30 /20%		
		30 /25%		
50	10		50	1.0/120
		30 /15%	55	
			60	
		25 /15%		
		30 /15%	60	
		35 /15%		

unit: nm

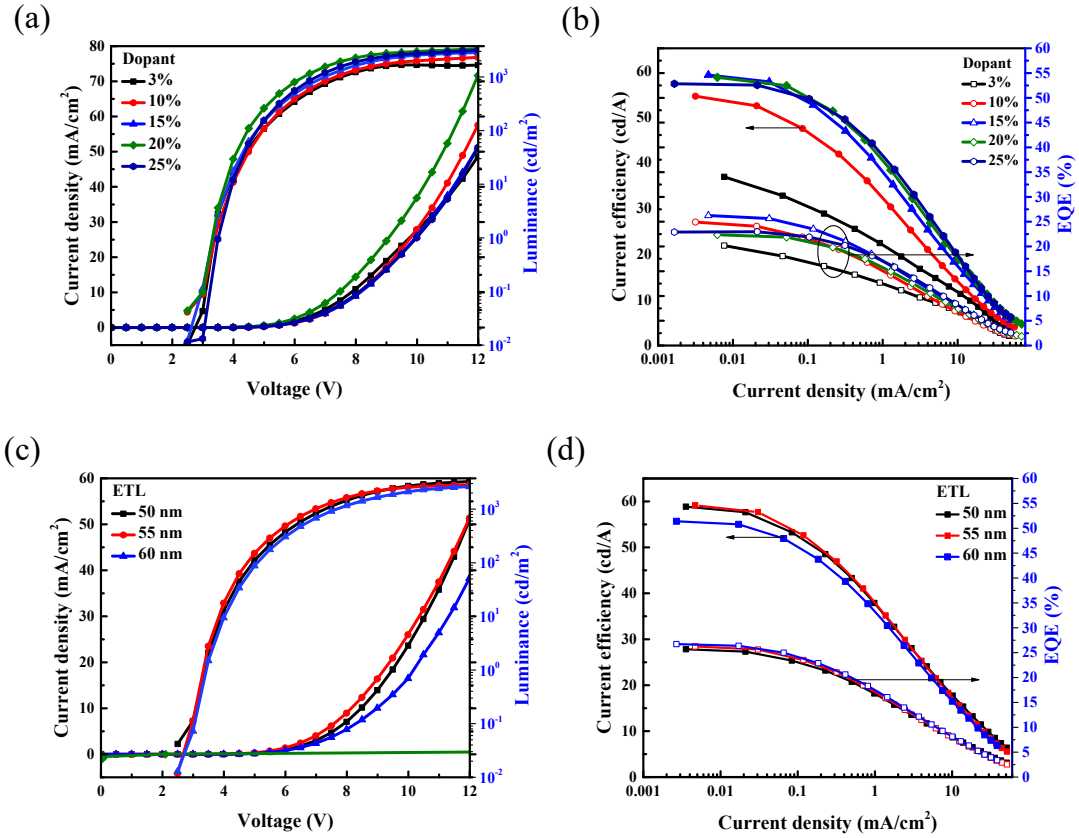

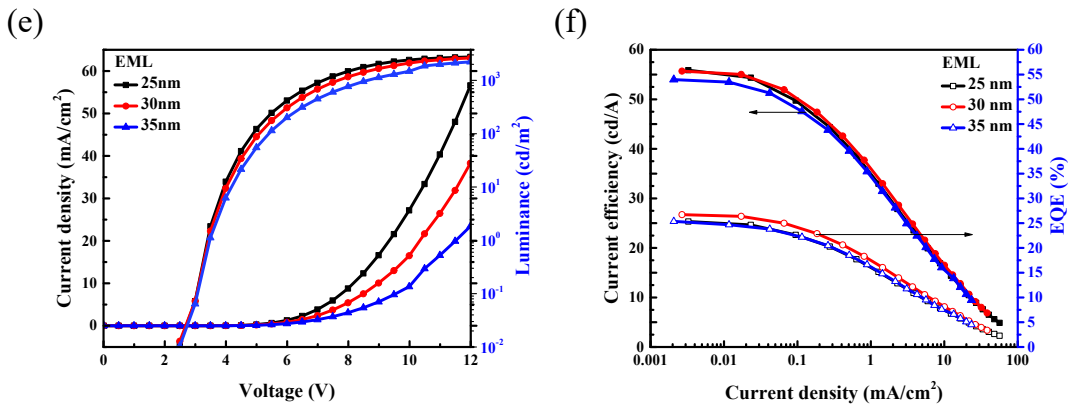

Figure S12. Device performance for OLEDs (a), (c), (e) J-L-V characteristics and (b), (d), (f) Efficiency-J-EQE. while **4SpAc35CzPy** with different dopant concentrations, ETL, and EML thickness, respectively.

Table S2. Device performance for OLEDs while **4SpAc35CzPy** with different dopant concentration, ETL, and EML thickness, respectively.

Device	V_{on} [a] (V)	CE [b] (cd/A)	PE [b] (lm/W)	EQE [b] (%)	*L* (nits)	CIE [c] (x, y)
3%	3.37	36.88	33.18	20.18	1677	(0.165,0.274)
10%	3.40	54.52	49.05	24.93	2327	(0.170,0.327)
15%	**3.33**	**59.16**	**53.24**	**26.25**	**2851**	**(0.179,0.365)**
20%	3.32	58.65	52.73	22.36	3366	(0.183,0.383)
25%	3.50	57.25	51.51	22.97	3156	(0.200,0.426)
ETL 50	3.37	58.86	52.93	25.69	3262	(0.178,0.366)
ETL 55	3.33	59.16	53.24	26.25	2678	(0.179,0.365)
ETL 60	**3.43**	**55.69**	**50.09**	**26.72**	**2627**	**(0.195,0.396)**
EML 25	3.40	55.88	50.26	25.32	2755	(0.187,0.380)
EML 30	**3.43**	**55.69**	**50.09**	**26.72**	**2627**	**(0.195,0.396)**
EML 35	3.47	53.98	48.56	25.36	2220	(0.206,0.408)

[a] measured at 1 cd/m^2; [b] measured at maximum; [c] measured at 9.5 V.

Table S3. The device lifetime of **4SpAc35CzPy** with different EML thickness.

Device	J=1 (mA/cm^2)#LT50
50 nm	32 (min) @362 nits
55 nm	36 (min) @333 nits
60 nm	40 (min) @368 nits

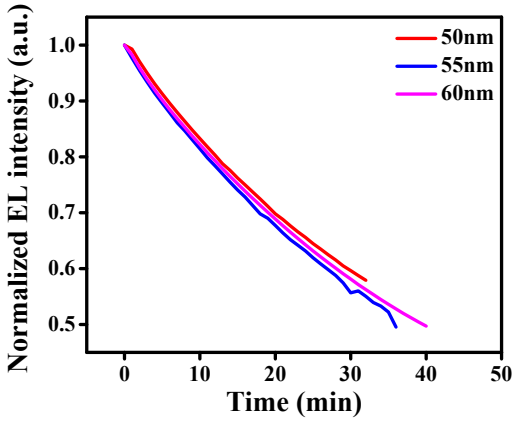

Figure S13. The lifetime curves for **4SpAc35CzPy** with different EML thicknesses.

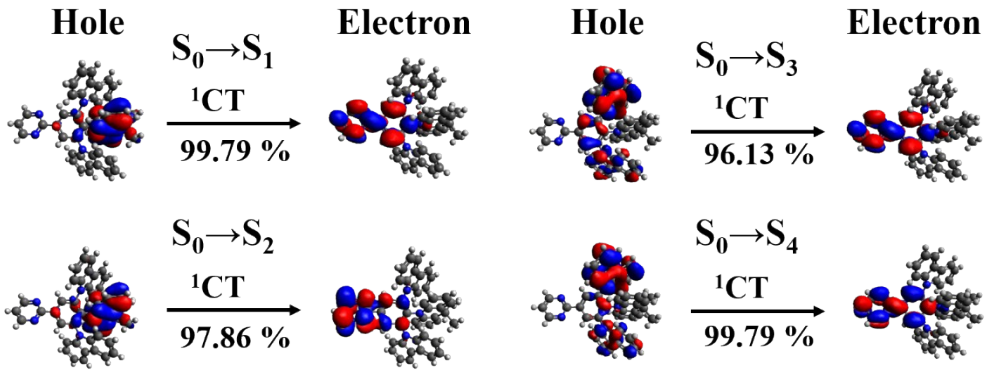

Figure S14. Natural Transition Orbitals (NTOs) of the Singlet excited states of **4Ac35CzPy**.

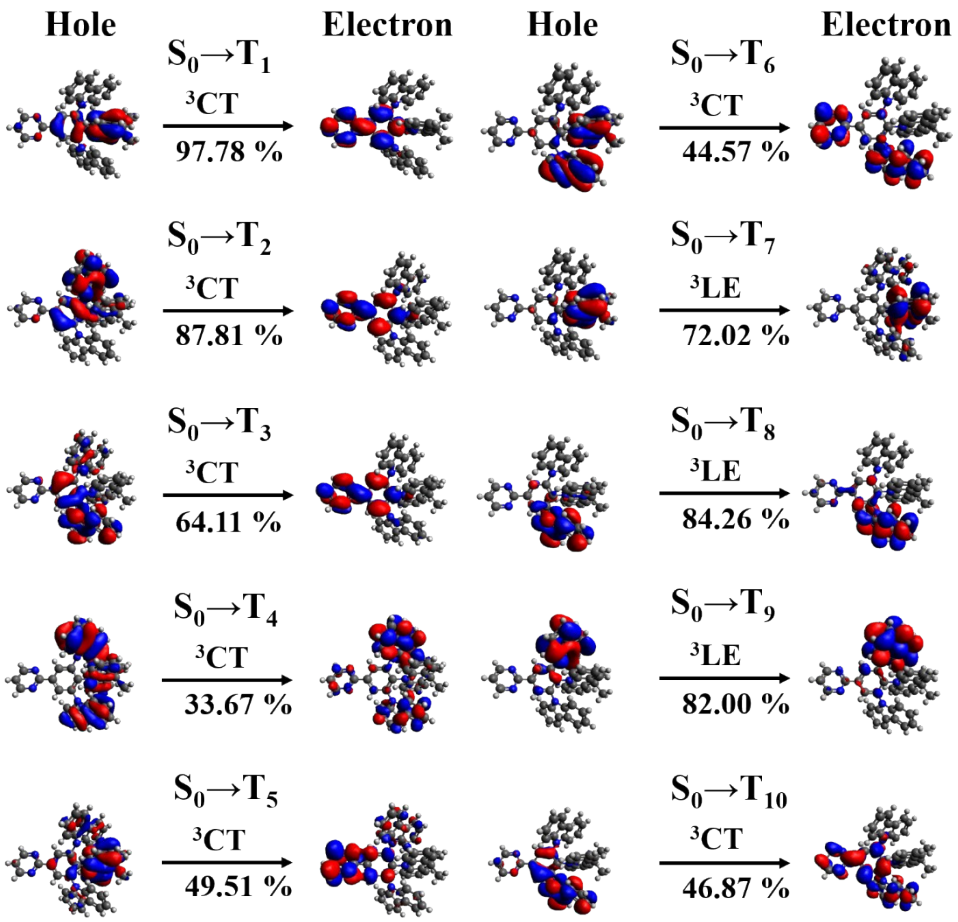

Figure S15. Natural Transition Orbitals (NTOs) of the Triplet excited states of **4Ac35CzPy**.

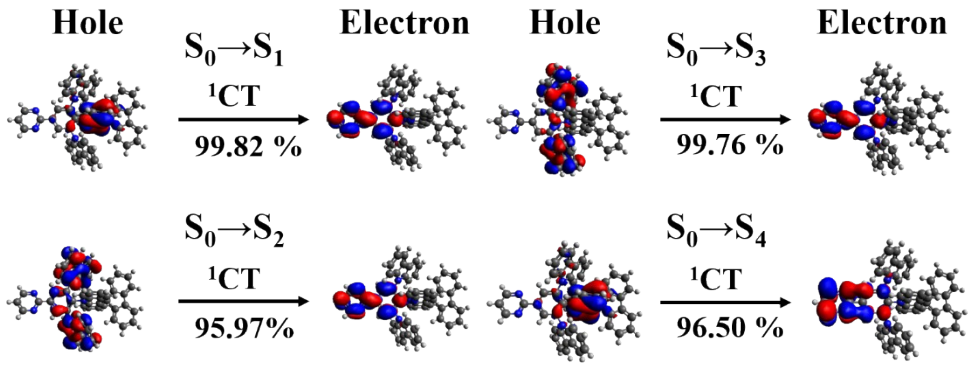

Figure S16. Natural Transition Orbitals (NTOs) of the Singlet excited states of **4SpAc35CzPy**.

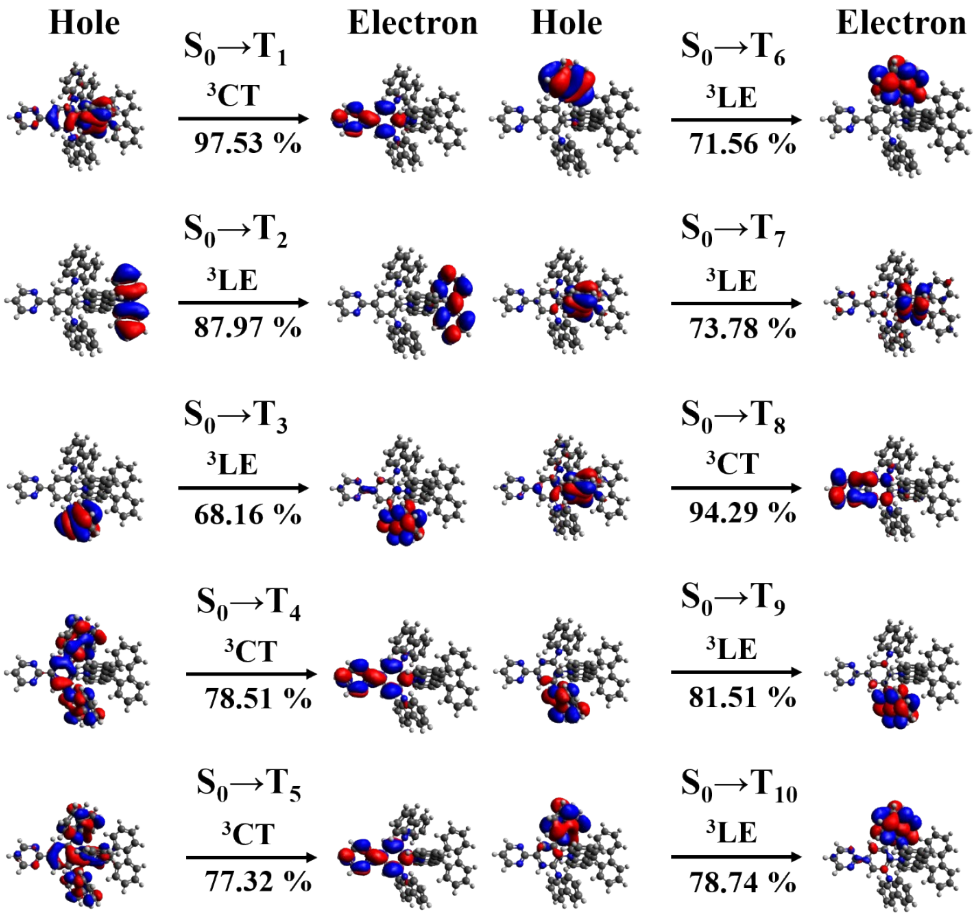

Figure S17. Natural Transition Orbitals (NTOs) of the Triplet excited states of **4SpAc35CzPy**.

Table S4. Spin-orbital Coupling (SOC) matrix constants (cm^{-1}) of **4Ac35CzPy**.

4Ac35CzPy					
$\langle S_n\|\hat{H}_{soc}\|T_n\rangle$	S_0	S_1	S_2	S_3	S_4
T_1	0.74	0.40	1.20	0.25	0.27
T_2	3.65	0.52	0.13	1.03	0.56
T_3	1.14	0.70	0.05	0.28	0.35
T_4	1.89	0.24	0.05	0.47	0.53
T_5	2.19	0.58	0.11	0.50	0.16
T_6	1.33	1.10	0.10	0.29	0.20
T_7	0.43	0.82	0.13	0.04	0.09
T_8	0.30	0.24	0.10	0.29	0.20
T_9	0.73	0.08	0.08	0.23	0.28
T_{10}	1.10	0.29	0.13	1.38	0.39

Table S5. Spin-orbital Coupling (SOC) matrix constants (cm^{-1}) of **4SpAc35CzPy**.

4SpAc35CzPy					
$\langle S_n\|\hat{H}_{soc}\|T_n\rangle$	S_0	S_1	S_2	S_3	S_4
T_1	0.89	0.43	0.48	0.25	1.13
T_2	0.21	0.01	0.00	0.00	0.01
T_3	0.51	0.27	0.15	0.33	0.02
T_4	1.71	0.39	0.16	0.90	0.09
T_5	3.04	0.36	0.99	0.06	0.27
T_6	2.88	0.38	0.73	0.17	0.26
T_7	0.57	1.03	0.07	0.11	0.20
T_8	0.53	0.97	0.07	0.16	0.19
T_9	0.56	0.70	0.15	0.18	0.10
T_{10}	0.69	0.30	0.29	0.38	0.05

Table S6. Summary of reported sky-blue OLED materials and their device performance parameters.

Name	η_{EQE}	η_{CE}	η_{PE}	**CIE**	**Year**
4SpAc35CzPy	25.7	58.7	52.9	(0.18,0.37)	2025
4SpAc35CzPy (3%)	20.2	36.9	33.2	(0.17,0.27)	2025
SpiroAC-TRZ	36.7	94	98.4	(0.18,0.43)	2016
MFAcPM	17.1	34.3	31.7	(0.16,0.21)	2017
Ac-PM	11.4	18.9	16.5	(0.15,0.15)	2017
2NPMAF	23.6	50.6	56.7	(0.19,0.34)	2018
3NPMAF	24.9	60.7	68.2	(0.20,0.40)	2018
25tCzBPym	23.3	65.5	51.1	(0.20,0.47)	2021
DPS-SAIA	19.3	30.4	18.1	(0.15,0.20)	2022
Me-DPS-SAIA	17.1	27.0	13.8	(0.14,0.16)	2022
CzmPPC	16.1	36.8	38.5	(0.16,0.27)	2022
***p,m*-SPAc-PPM**	25.1	58.2	50.7	(0.20,0.36)	2022
4Ac35CzPy	21.2	53.3	48.1	(0.19,0.40)	2023
2,7-CF3-Ph-DMAC-TRZ	22.5	55.1	55.8	(0.22,0.41)	2024
PCzoTrz	24.6	53.5	-	(0.16,0.36)	2024
HCB-1	21.0	48.1	30.2	(0.18,0.36)	2025

Reference:

[1] Y.-Z. Li, H.-C. Liang, C.-H. Chen, C.-H. Chiu, B.-Y. Lin, J.A. Tan, J.-H. Lee, T.-L. Chiu, M.-k. Leung, Modification of thermally activated delayed fluorescence emitters comprising acridan–pyrimidine moieties for efficient sky-blue to greenish-blue OLEDs, J. Mater. Chem. C 11(41) (2023) 14395-14403.